RSC Advances

PAPER

Cite this: *RSC Adv.*, 2022, **12**, 10915

Enhanced fluorescence quenching for *p*-nitrophenol in imidazolium ionic liquids using a europium-based fluorescent probe†

Sijing Yi, * Huanhuan Li and Xiaoxia Liu

p-Nitrophenol (PNP) is a toxic contaminant in water, the detection of which has attracted considerable attention. Since ionic liquids (ILs) have been widely used as popular solvents in both extraction and catalysts for PNP, the remediation of PNP is not limited to water and traditional organic solvents. Thus, it is significant to develop approaches for the detection of PNP in ILs. Accordingly, the present work is focused on the detection of PNP in a series of imidazolium-based ILs, 1-hexyl-3-methyl-imidazolium bromide ([Hmim]Br), 1-butyl-3-methyl-imidazolium tetrafluoroborate ([Bmim]BF_4), 1-butyl-3-methyl-imidazolium trifluoromesulfonate ([Bmim]TfO), 1-butyl-3-methyl-imidazolium trifluoroacetate ([Bmim]TA), and 1-butyl-3-methyl-imidazolium nitrate ([Bmim]NO_3), using a europium-based fluorescent probe, Na_3[Eu(DPA)$_3$] (DPA = 2, 6-pyridinedicarboxylic acid). This fluorescent probe showed excellent selectivity and sensitivity toward [Bmim]NO_3 in aqueous solution. Further studies showed that not only the fluorescence performance of the europium complex was enhanced in the other four ILs compared with that in water, but also the detecting capability for PNP was improved. The order of the quenching efficiency in different solvents was: [Bmim]BF_4 > [Bmim]TfO > [Hmim]Br > [Bmim]TA > water. The higher sensitivity for PNP in ILs was proven to be related to the efficient energy transfer of the europium complex and lower solvent polarity of the ILs. The quenching mechanism for the detection of PNP was established as being due to the ground state electrostatic interactions between the fluorescent probe and analyte, photoinduced electron transfer (PET) and inner filter effect (IFE).

Received 13th January 2022
Accepted 24th March 2022

DOI: 10.1039/d2ra00251e

rsc.li/rsc-advances

1. Introduction

Phenolic compounds of *p*-nitrophenol (PNP) have played important roles in many fields, such as in explosives, dyes, pesticides, and pharmaceuticals.[1,2] However, it is also a serious source of pollution for groundwater and soil, and has been labeled as a highly toxic compound due to the mutagenic and carcinogenic effects it has on the main organs of the human body.[3–5] To deal with these issues, scientific researchers have been motivated to develop effective detection and treatment techniques, such as chromatography, spectrometry, and electrochemical sensors.[6,7] Among these various detection techniques, fluorescence quenching chemosensing technology based on a donor–acceptor electron transfer mechanism has been regarded as one of the most promising approaches by virtue of its high sensitivity, quick response and convenience of use.[8–10] In the field of fluorescence chemosensors, lanthanide-based fluorescent probes for nitro compound detection have been a topic of interest due to their unique fluorescence properties, such as large Stokes shifts, good fluorescence monochromaticity, millisecond-level fluorescence lifetimes, and visible light emission.[11–13] Moreover, it is worth noting that the detection capability of fluorescent probes has proven to be highly dependent on the solvent used, which is sensitively reflected in the corresponding quenching efficiency and limit of detection (LOD).[14–17] However, the detection of PNP with lanthanide-based fluorescent probes remains limited to the aqueous phase and traditional organic solvents.

Recently, ionic liquids (ILs) as innovative fluids have been widely acclaimed due to their excellent physicochemical properties, including nonflammability, excellent thermal stability, low combustibility, and high ionic conductivity.[18,19] They have shown great promise to be an alternative to conventional solvents in the fields of catalysis,[20] electrochemical analysis,[21] and wastewater treatment,[22–24] especially in the extraction of organic compounds. The progress in IL science inevitably means that the exposure of PNP and their derivatives is not limited to water and traditional organic solvents. For instance, the removal efficiency of PNP in wastewater has been shown to be improved significantly using ILs,[25–29] and metal nanoparticles used for the catalytic reduction of nitrophenol have

Department of Basic Science, Shanxi Agricultural University, Taigu, 030801, China. E-mail: yisijing@139.com; Tel: +86 354 6288341

† Electronic supplementary information (ESI) available: Details on the calculation method of the luminescence parameters and luminescence decay curves of Eu[III] in different solvents. Emission spectra of fluorescence titration and UV-vis absorption spectra of PNP in different solvents. See DOI: 10.1039/d2ra00251e

been shown to be stabilized and size-controlled by ILs.[30–35] Consequently, the detection of nitro compounds in ILs has become a reality, and it is thus significant to investigate the potential influence of ILs on the fluorescence and response performance of fluorescent probes. At the same time, ILs have been recognized as an ideal media for the study of lanthanide luminescence properties owing to their favorable spectral properties, such as no interference in visible spectral regions and the obviously enhanced fluorescence properties of lanthanide compounds in ILs.[36–39] Benefiting from the potential hydrogen bond formation between ILs and ligands of lanthanide complexes, improvements in both luminescence efficiency and stability have been achieved.[40,41] It is expected that the use of ILs as solvents might bring about improved fluorescence and detection ability of lanthanide-based fluorescent probes. However, to the best of our knowledge, related studies have been scarcely reported.

Inspired by this, here we selected a series of imidazolium ILs (Fig. 1a): 1-butyl-3-methyl-imidazolium tetrafluoroborate ([Bmim]BF_4), 1-hexyl-3-methyl-imidazolium bromide ([Hmim]Br), 1-butyl-3-methyl-imidazolium trifluoromethansulfonate ([Bmim]TfO), 1-butyl-3-methyl-imidazolium trifluoroacetate ([Bmim]TA), and 1-butyl-3-methyl-imidazolium nitrate ([Bmim]NO_3) to clarify the specific solvent effect on the detection performance of the europium-based fluorescent probe. ILs with imidazolium as cations were chosen here not only because they have been extensively applied in the extraction, reduction and analysis of PNP,[23,25–35] but also because they provide an ideal solvent environment to improve the fluorescence properties of europium complexes.[42–45] In the course of better detection performance, we synthesized the lanthanide complex Na_3[-Eu$(DPA)_3$] (abbreviated as Eu[III], DPA = 2,6-pyridinedicarboxylic acid; Fig. 1b) as a fluorescent probe. A desirable fluorescence intensity was obtained as a result of saturated coordination of DPA ligands to the Eu^{3+} ion.[46–50] Enhanced detection capability of this fluorescent probe was achieved using ILs as a solvent, and the underlying mechanism of sensing behavior towards PNP was also explored. It is hoped that our research results will provide guidelines for scientific research on the detection of nitro compounds in ILs and promote the further application of ILs.

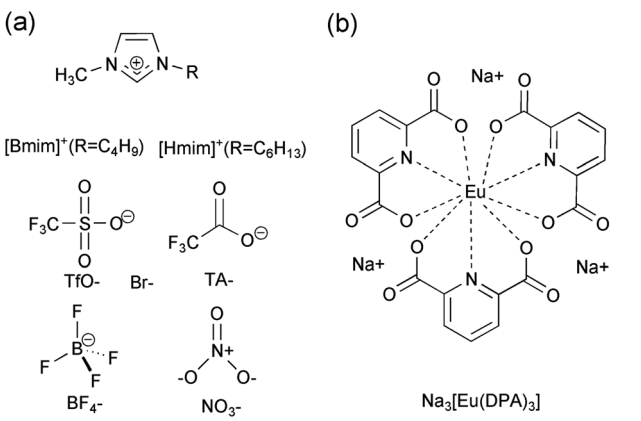

Fig. 1 (a) Chemical structure of cations and anions of the selected ionic liquids and (b) the europium complex Na_3[Eu$(DPA)_3$].

2. Experimental section

2.1. Materials

Eu$(NO_3)_3 \cdot 6H_2O$ (99.9%) and 2,6-pyridinedicarboxylic acid ($DPAH_2$, 99%) were purchased from Alfa Aesar and used as received. PNP (99%) was purchased from Guangfu Fine Chemical Research Institute (Guangfu Chemical Co., Tianjin, China). Room-temperature ionic liquids (ILs, ≥ 99.0%), were purchased from the Center for Green Chemistry and Catalysis, LICP, CAS. The other chemical reagents were of analytical grade.

2.2. Synthesis of europium complexes

The europium complexes, Na_3[Eu$(DPA)_3$] (abbreviated as Eu[III]) were synthesized as follows. A mixture of the $DPAH_2$ (5.010 g, 0.03 mol) and NaOH (2.400 g, 0.06 mol) was dissolved in 60 mL of distilled water and incubated at 90 °C for 1 h. Then, an aqueous solution of Eu$(NO_3)_3 \cdot 6H_2O$ (4.459 g, 0.01 mol) was added dropwise along with continuous stirring for another 2 h. The reaction solution was cooled to room temperature and kept under these conditions for 24 h. After that, most of the solvent was removed by a rotary evaporator. The obtained product was recrystallized from hot water with a solid/liquid ratio of 1/2.25. The final materials were obtained in a yield of *ca.* 86% after being dried in a vacuum oven at 50 °C for 24 h. Elemental analysis calculated for Eu[III] ($C_{21}H_9N_3O_{12}Na_3 \cdot$Eu, %): C, 35.21; H, 1.27; N, 5.87. Found (%): C, 35.28; H, 1.15; N, 5.47.

2.3. Fluorescence quenching titration of PNP

To obtain solutions for fluorescence and UV-vis measurements, aqueous solutions of 25 mg mL^{-1} Eu[III] and 0.40 mM of PNP were first prepared. Then, a series of 1 mg mL^{-1} Eu[III] solutions with different concentrations of PNP in different solvent systems were obtained by mixing the as-prepared two solutions and ILs in the designated proportions. The ILs used in this study are all hydrophilic and remained liquid at room temperature. All the samples were treated by ultrasonication for 30 min before the tests. Each titration was repeated 3 times to achieve concordant values. The quenching percentage (Q) was calculated using eqn (1):

$$Q = (I_0 - I)/I_0 \times 100\% \quad (1)$$

where I_0 and I are the fluorescence intensity values before and after the addition of the analyte, respectively.

2.4. Characterization

Elemental analyses for C, H and N were performed on a Vario MACRO Cube Elemental analyzer. The excitation and emission spectra of all samples were recorded using a RF-5301 PC Shimadzu spectrofluorometer (xenon lamp, 150 W). The slit width for all samples was set as 1.5 nm for both the excitation and emission. The luminescence lifetimes were recorded on Edinburgh Instruments FLS920 apparatus using a μF920

microsecond flash lamp as excitation source and monitoring the luminescence intensity decay according to the time of the $^5D_0 \rightarrow {}^7F_2$ transition. UV-vis spectra of the solutions were measured using a Shimadzu UV-3600 spectrophotometer.

3. Results & discussion

3.1. Effect of ionic liquids on the fluorescence properties of the europium complex

The fluorescence properties of europium complexes are very sensitive to the chemical microenvironment. Therefore, the fluorescence spectra of Eu[III] in different ILs were studied here. Fig. 2 shows the fluorescence excitation and emission spectra of Eu[III] in water and different ILs. As shown in Fig. 2a, the maximum excitation peak is located at 288 nm when Eu[III] was dispersed in water, which was attributed to the antenna effect generated by the energy transfer from DPA to Eu^{3+}.[51] This peak was noticeably red-shifted from 288 to 293 nm ([Bmim]TA, [Bmim]TfO, and [Bmim]BF_4) and 302 nm ([Hmim]Br) when Eu[III] was dispersed in the ILs. This could be attributed to the reduction of covalency of the Eu–O bonds in the europium complexes, indicating that the energy transfer from DPA to the central Eu^{3+} ion was affected by the ILs.[52]

As shown in the emission spectra of Eu[III] in different solvents upon excitation at their corresponding excitation wavelengths (Fig. 2b), characteristic emission bands associated with the $^5D_0 \rightarrow {}^7F_J$ ($J = 0$–4) transition of the central Eu^{3+} ion could be observed in the range of 570–720 nm.[53] It should be noted that not only the relative intensity of the different transitions changed, but also the peak shapes of the bands were changed in different solvents, especially the emission bands corresponding to the $^5D_0 \rightarrow {}^7F_1$ transition. Such variations indicated that the coordination sphere of the Eu^{3+} ion was affected by the ILs and different symmetry classes occupied by Eu^{3+} in the europium complexes.[54] As is well known, the intensity ratio of $^5D_0 \rightarrow {}^7F_2$ to $^5D_0 \rightarrow {}^7F_1$ transitions is closely related to the chemical environment around the Eu^{3+} ion.[55] The values of the intensity ratio, η, can thus be used to measure the degree of asymmetry in the Eu^{3+} coordination sphere.[56] A higher intensity ratio usually implies a lower symmetry of the coordination sphere. The η values of Eu[III] in different solvents were calculated and are listed in Table 1. As shown in Table 1, all the η values of Eu[III] dispersed in ILs decreased compared to that in water, indicating the higher coordination symmetry of the Eu^{3+} complex. In addition, the luminescence decay curves recorded for the $^5D_0 \rightarrow {}^7F_2$ emission of Eu[III] dispersed in different solvents could be well fitted to a single exponential function (Fig. S1†). This indicated no dissociation of the europium complexes occurred and that only one europium site was present in water or the ILs.[57] Furthermore, the lifetime values (τ) of Eu[III] obtained in ILs were all relatively longer than that in water, reflecting a more efficient energy transfer between the DPA ligands and Eu^{3+} ions. This could also be proved from the decreased nonradiative rate constant (k_{nr}) value of Eu[III] in the ILs (Table 1), which was calculated using eqn (S1) and (S2) listed in the ESI.† The lowest k_{nr} value was obtained in the IL [Bmim]BF_4, indicating that a comparatively efficient radiative relaxation process occurred in this IL compared to in the other solvents.

The influence of ILs on the coordination sphere was mainly attributed to the hydrogen bond interactions of the imidazolium ions in the ILs with Eu[III].[40,58] As ideal H-bond donors, the hydrogen atoms of the C–H bonds on the aromatic rings of the imidazolium cations form hydrogen bonds with the carboxyl groups of the DPA ligands. This is beneficial to decreasing the

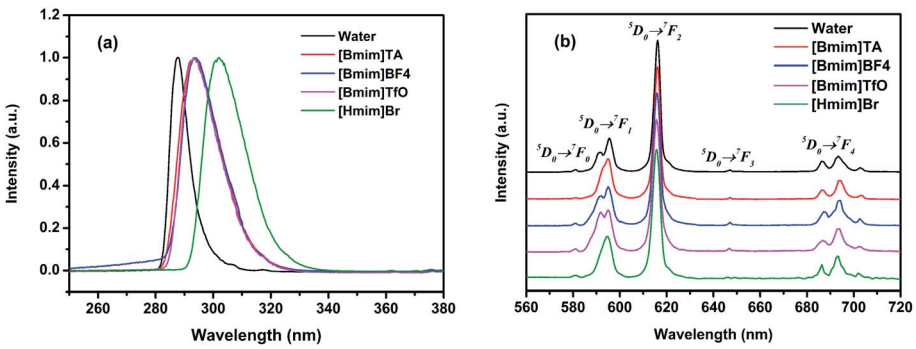

Fig. 2 (a) Excitation and (b) emission spectra of Eu[III] in water and different ILs. The spectra were normalized to the most intense peak and $^5D_0 \rightarrow {}^7F_2$ transition, respectively.

Table 1 The intensity ratio of $^5D_0 \rightarrow {}^7F_2$ to $^5D_0 \rightarrow {}^7F_1$ transitions (η), lifetimes (τ) and nonradiative rate constants (k_{nr}) of Eu[III] in different solvents

Types of solvent	Water	[Bmim]BF_4	[Hmim]Br	[Bmim]TfO	[Bmim]TA
η	4.23	3.19	3.84	3.86	3.98
τ/ms	1.50	2.38	1.98	1.87	1.86
k_{nr}/ms^{-1}	0.299	0.100	0.159	0.183	0.186

nonradiative transition deactivation of the europium complexes and results in a more effective energy transfer efficiency.

Additionally, the fluorescence intensities of Eu[III] were found to also greatly depend on the types of ILs. As shown in Fig. 3a, the emission intensity recorded at 616 nm in different solvents at the same Eu[III] concentration varied as follows: [Bmim]TA > water > [Bmim]BF_4 > Bmim]TfO > [Hmim]Br > [Bmim]NO_3. It was noteworthy that the fluorescence intensity was found to be almost completely quenched when the Eu[III] complex was dispersed in [Bmim]NO_3. Such solvent-dependent luminescent properties can be applied to the sensing of ILs containing nitro groups. Therefore, the emissive response was first investigated by gradually titrating an aqueous solution of Eu[III] with [Bmim]NO_3. As shown in Fig. 3b, the fluorescence intensity of Eu[III] decreased significantly with the addition of [Bmim]NO_3, and was almost undetectable when the [Bmim]NO_3 content reached 15 vol%. The decay dynamics of the emission band at 616 nm could be well fitted using an exponential equation ($y = 548.34\ e^{-49.32x}$, $R^2 = 0.999$, see the inset in Fig. 3). Moreover, the luminescence lifetimes of Eu[III] remained almost unchanged in the absence and presence of [Bmim]NO_3 (Fig. S2†), suggesting that the quenching of the emission intensity can be attributed to the non-emission ground state formed between the nitrate ions of [Bmim]NO_3 and the DPA ligands of Eu[III] rather than the central Eu^{3+} ions.[59,60] Such luminescent quenching properties imply that the europium complexes can be applied sense molecules that contain nitro groups.

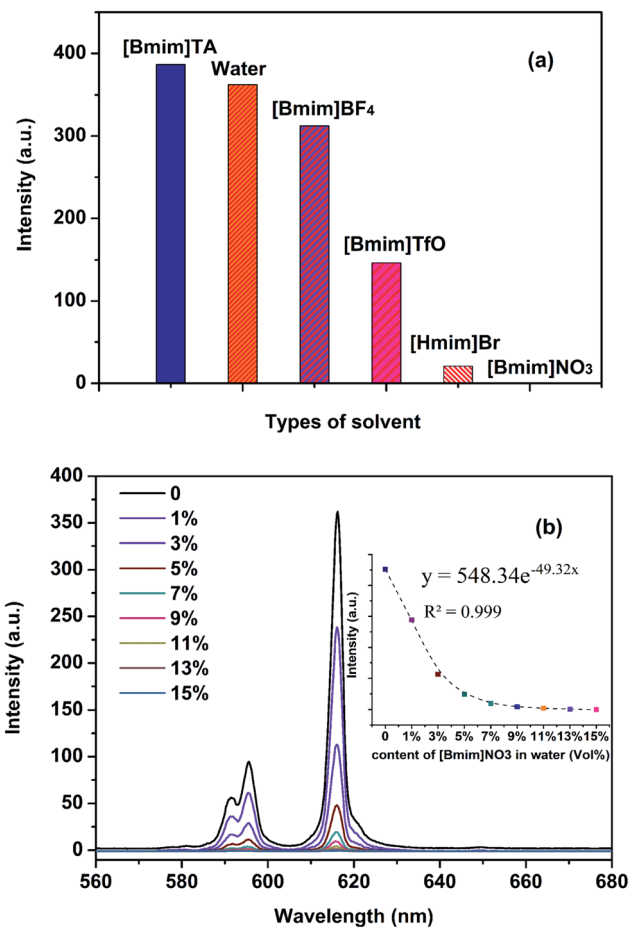

Fig. 3 (a) Emission intensity of Eu[III] at 616 nm in water and different ILs. (b) Fluorescence titration of Eu[III] dispersed in aqueous solutions containing different [Bmim]NO_3 content, where the inset shows the quenched emission intensity of Eu[III] recorded at 616 nm.

3.2. Effect of the type of ionic liquid on the detection performance

On the basis of the fluorescence quenching effect of Eu[III] on molecules containing nitro groups, a batch of Eu[III] dispersed in water and ILs was investigated to explore the fluorescence response to PNP and the corresponding influence of the ILs. Since the emission intensity of Eu[III] was completely quenched in [Bmim]NO_3, the PNP detection was only conducted in the other four ILs. As shown in Fig. 4, all the fluorescence intensities of Eu[III] were significantly decreased after adding PNP with a concentration of 0.18 mM, and the quenching percentage differed according to the types of ILs. The results showed that the fluorescence of Eu[III] in the different solvents was the following descending order: [Bmim]BF_4 (86.3%), [Hmim]Br (84.3%), [Bmim]TfO (84.2%), [Bmim]TA (82.6%), and water (72.8%). Compared with that in water, the europium complexes dispersed in the ILs showed more sensitive detection for PNP with relatively higher quenching percentages.

To examine the PNP-detecting sensitivity of Eu[III] in different solvents in detail, fluorescence quenching titrations of PNP were carried out to monitor the emissive response (Fig. 5a and S3†). By gradually increasing the concentration of the analyte, the detected fluorescence intensity decreased continuously. The quenching efficiency was quantitatively analyzed using a Stern–Volmer equation (eqn (2)):

$$(I_0/I) = K_{sv}[A] + 1 \quad (2)$$

where K_{sv} is the Stern–Volmer quenching constant, which is usually used to allow a comparison of the quenching efficiency, and [A] is the concentration of the analyte (PNP). Fig. 5b shows the Stern–Volmer curves for Eu[III] obtained by plotting I_0/I

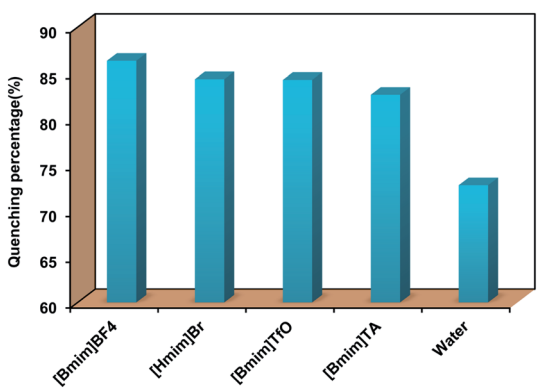

Fig. 4 Quenching efficiency of the fluorescence of Eu[III] dispersed in water and different types of ILs after the addition of PNP (0.18 mM).

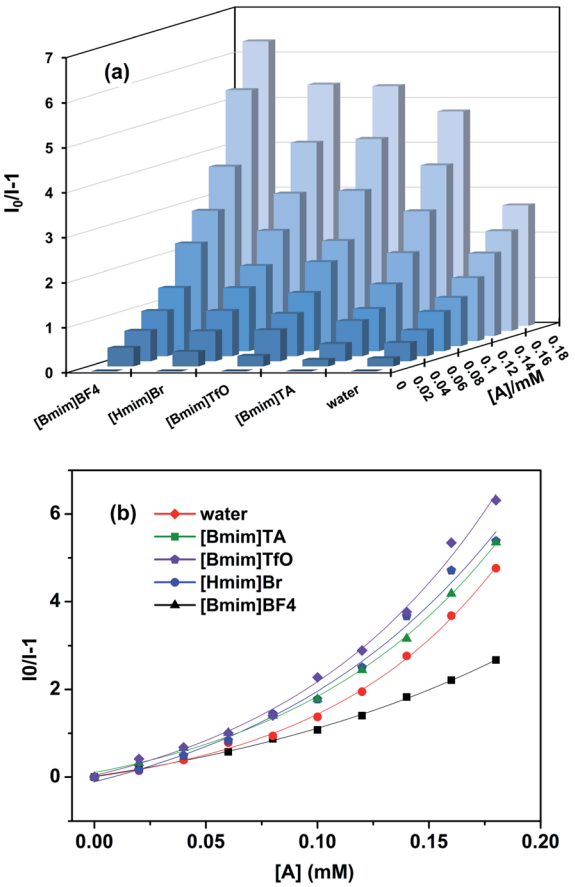

Fig. 5 (a) Fluorescence titration of Eu[III] with the incremental addition of PNP in water and different types of ILs. (b) Stern–Volmer plots of I_0/I *versus* [A] (the PNP concentration) in water and the different ILs.

versus [A]. All the Stern–Volmer curves are almost linear at low concentration ranges (from 0.02 to 0.10 mM), but subsequently deviate from linearity and curve upwards at higher concentrations. The linear fitting equations at low concentration ranges are listed in Table 2. The nonlinear and upward curves at higher concentrations suggested that the fluorescence quenching mechanism could be attributed to the presence of simultaneous static and dynamic quenching.[15,59,60]

Furthermore, the LOD was also calculated using eqn (3), which can be used to ascertain the lowest concentration of the analyte that can be reliably measured:

$$\mathrm{LOD} = 3 \times \sigma / K_{sv} \quad (3)$$

where σ is the standard deviation of the blank group. The calculated values of K_{sv} and the LOD values for PNP in different solvents are listed in Table 2, which are comparable with other europium-based sensors reported to date (Table S1†). As a result, the K_{sv} values of Eu[III] dispersed in the ILs were all higher than that in water. The highest K_{sv} value ($1.97 \times 10^4\ M^{-1}$) was obtained using [Bmim]BF_4, while the lowest LOD (3.29×10^{-6} M) was obtained using [Hmim]Br. These results confirmed that europium complexes dispersed in ILs have more efficient detection performance than that in water.

Based on the above experimental results, the detection performance of the fluorescent probe was improved when Eu[III] was dispersed in the ILs, and the quenching efficiencies were enhanced in the same order as that of the energy transfer efficiency of Eu[III]. The highest quenching percentage and K_{sv} value obtained in [Bmim]BF_4 corresponded to the longest lifetime and lowest k_{nr} value of Eu[III]. This indicated that the energy transfer effect of the europium complexes played an important role in the fluorescence detection efficiency. To confirm our speculation, the effect of the appropriate addition of ILs on the detection performance was further investigated. Since the peak shape and position were found to broaden and right shift in the fluorescence spectra of Eu[III] when the IL content was higher than 10%, aqueous solutions with 10% IL content were selected to study the influence of the IL type on the fluorescence detection performance.

Fig. S4† shows the fluorescence excitation and emission spectra of Eu[III] dispersed in water and aqueous solutions containing 10% ILs, wherein no obvious changes could be observed in the shape and position of the excitation and emission bands. This indicated that the coordination environment of Eu^{3+} remained unchanged when the europium complexes were dispersed in aqueous solutions with an ionic liquid content of 10%. All the η values in 10% ILs obtained from $^5D_0 \rightarrow {}^7F_2$ to $^5D_0 \rightarrow {}^7F_1$ transitions were around 4.2, indicating the similar asymmetry degree of the Eu^{3+} coordination sphere. In addition, the τ values of Eu[III] dispersed in 10% ILs were very close to that in water, which were 1.50, 1.46, 1.44 and 1.59 ms for 10%[Bmim]TA, 10%[Bmim]TfO, 10%[Bmim]BF_4, and 10% [Hmim]Br, respectively (Fig. S5†). These results also reflected the similar energy transfer process of Eu[III].

With the addition of 0.18 mM of PNP, all the fluorescence intensity values were significantly decreased, and the quenching degree differed according to the types of the ILs. As shown in Fig. 6, the quenching percentages were all unexpectedly decreased when Eu[III] was dispersed in aqueous solutions containing 10% ILs. The fluorescence quenching percentage of Eu[III] in the different solvents was in a descending order as follows: water (72.8%), 10%[Bmim]BF_4 (72.0%), 10%[Hmim]Br (71.2%), 10%[Bmim]TfO (64.9%), 10%[Bmim]TA (47.3%). Furthermore, the europium complex dispersed in an aqueous solution containing 10%[Bmim]TA showed the lowest quenching percentage.

The sensing sensitivities towards PNP of Eu[III] in different solvents was also investigated by conducting in-depth

Table 2 Summary of the equation fitting of Stern–Volmer curves, correlation coefficients (R^2), quenching constants (K_{sv}) and limit of detection (LOD) values for the fluorescence titration of Eu[III] toward PNP in different solvents

Types of solvent	Fitting equation	R^2	K_{sv} (M^{-1})	LOD (M)
Water	$I_0/I = 10\,795[A] + 1$	0.992	1.08×10^4	8.43×10^{-6}
[Bmim]BF_4	$I_0/I = 19\,726[A] + 1$	0.998	1.97×10^4	4.48×10^{-6}
[Hmim]Br	$I_0/I = 17\,431[A] + 1$	0.999	1.78×10^4	3.29×10^{-6}
[Bmim]TfO	$I_0/I = 18\,537[A] + 1$	0.995	1.84×10^4	6.62×10^{-6}
[Bmim]TA	$I_0/I = 12\,179[A] + 1$	0.987	1.22×10^4	9.90×10^{-6}

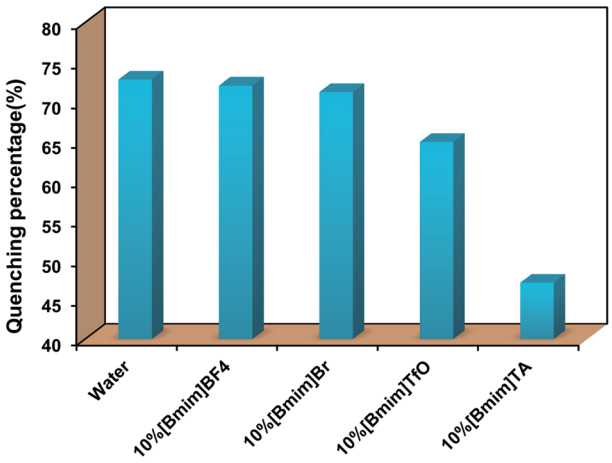

Fig. 6 Quenching efficiency of the fluorescence intensity of Eu[III] dispersed in water and aqueous solutions containing different types of ILs after the addition of PNP (0.18 mM).

fluorescence quenching titrations (Fig. 7a). Upon gradually increasing the PNP content, the detected fluorescence intensity decreased correspondingly. The Stern–Volmer curves given by the plots of I_0/I *versus* PNP concentration are shown in Fig. 7b. Except for a global linear fitting of [Bmim]TA, all the other Stern–Volmer curves of aqueous solutions containing ILs exhibit a good linear relationship in the range of 0–0.10 mM PNP concentrations, and exhibit nonlinear curves when the PNP concentration is higher than 0.10 mM (Fig. S6†). This also reflected that the fluorescence quenching mechanism could be attributed to the presence of both static and dynamic quenching at high PNP concentrations ([A] > 0.10 mM). In addition, it can also be speculated that static quenching was dominant in the [Bmim]TA solvent system because linear fitting was achieved across the entire PNP concentration range. The calculated K_{sv} and LOD values for PNP in aqueous solutions containing the different ILs are also listed in Table 3. The K_{sv} values were all decreased somewhat in aqueous solutions containing ILs in comparison to in water (1.08×10^4 M^{-1}). The highest K_{sv} value (9.92×10^3 M^{-1}) and the lowest LOD (6.56×10^{-6} M) were obtained using an aqueous solution containing 10%[Bmim]BF_4. The decreased detection performance of Eu[III] dispersed in aqueous solutions containing the 10% ILs demonstrated that the changed coordination sphere and enhanced energy transfer efficiency of Eu[III] in the pure ILs played an important role in the quenching process. Furthermore, the lower quenching efficiencies obtained in 10% ILs implied that other factors also potentially affect the quenching process.

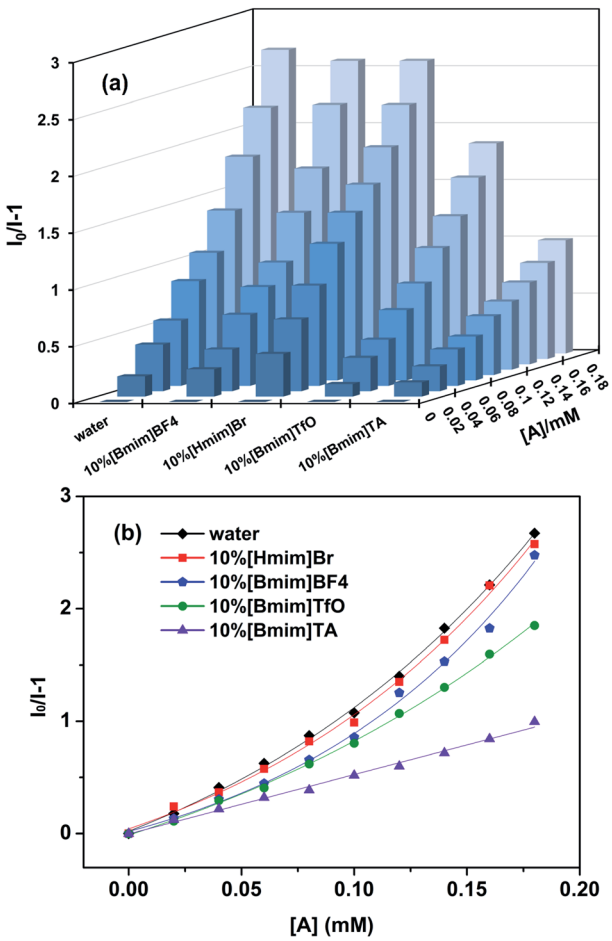

Fig. 7 (a) Fluorescence titration of Eu[III] with the incremental addition of PNP in water and aqueous solutions with different ILs. (b) Stern–Volmer plots of I_0/I *versus* [A] (the PNP concentration) in water and aqueous solutions with different ILs.

3.3. Mechanism of fluorescence quenching

According to the non-linear Stern–Volmer curves obtained from the fluorescence titrations of PNP, multiple mechanisms are involved in the quenching process. The following three reasons can account for the quenching mechanism, which is shown in Fig. 8a. The first reason is the static quenching caused by the electrostatic interactions between the free Lewis-base site of the fluorophore (unsaturated pyridine nitrogen of the DPA ligand) and the hydroxyl group of PNP. This interaction could form a non-emission ground state and result in a quenching effect.[15,60,61] Another reason can be attributed to the dynamic quenching mechanism caused by a collisional encounter between the excited state of the fluorescent probe and PNP, which is accompanied by electron transfer and results in fluorescence quenching. As a result of the conduction band (CB) energy level of Eu[III] being higher than the lowest unoccupied molecular orbitals (LUMOs) of PNP, excited electrons are typically transferred from the CB of Eu[III] to the LUMOs of PNP upon excitation.[12,15] Electron-deficient PNP could present

Table 3 Summary of the fitting equations of Stern–Volmer curves, correlation coefficients (R^2), quenching constants (K_{sv}) and limit of detection (LOD) values for the fluorescence titration of Eu[III] toward PNP in aqueous solutions containing different ILs

Types of solvent	Fitting equation	R^2	K_{sv} (M^{-1})	LOD (M)
10%[Bmim]BF_4	$I_0/I = 9917.4[A] + 1$	0.995	9.92×10^3	6.56×10^{-6}
10%[Hmim]Br	$I_0/I = 8569.4[A] + 1$	0.993	8.57×10^3	7.47×10^{-6}
10%[Bmim]TfO	$I_0/I = 8091.2[A] + 1$	0.991	8.09×10^3	8.86×10^{-6}
10%[Bmim]TA	$I_0/I = 4710.1[A] + 1$	0.991	4.71×10^3	1.08×10^{-5}

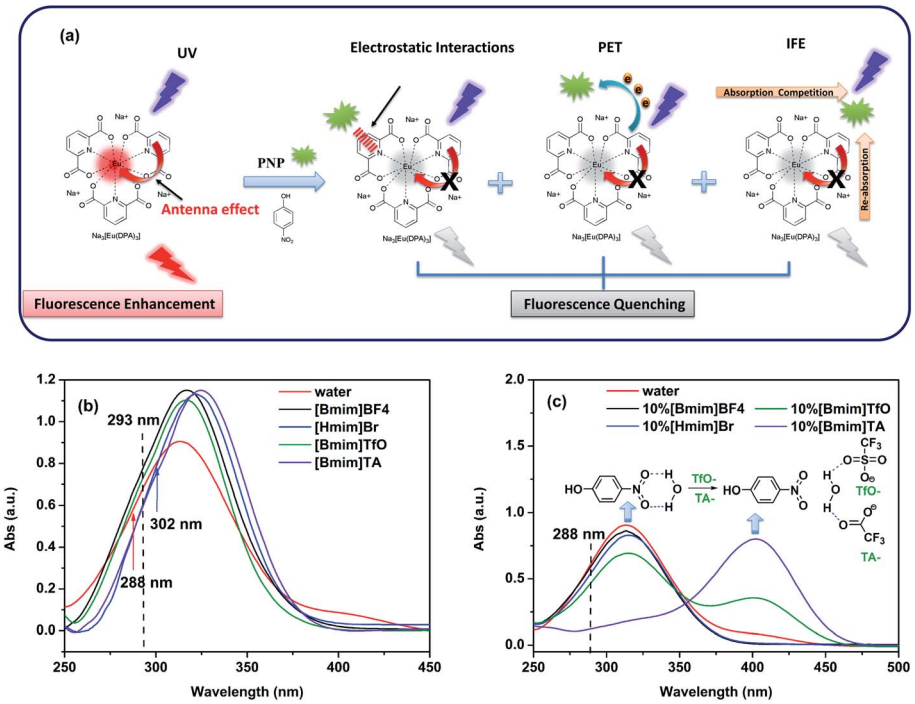

Fig. 8 (a) Schematic presentation of the multi quenching mechanism of Eu[III] by PNP. (b) UV-visible spectra of PNP dispersed in water and different ILs and (c) aqueous solutions containing 10% IL.

a lower LUMO energy level due to the electron-withdrawing ability of its nitro group, thus meaning that excited electrons are more easily transferred to the PNP molecules.[62,63] Thereby, the fluorescence quenching of Eu[III] can be observed upon the addition of PNP due to photoinduced electron transfer (PET) between Eu[III] and PNP.

Moreover, the competitive absorption of the excitation and emission radiation of the DPA ligands by PNP could also lead to fluorescence quenching, which is well-known as an inner filter effect (IFE).[12,61–63] As is known, the DPA ligand transfers energy to the central Eu^{3+} ion, subsequently resulting in the enhanced fluorescence emission of the europium complexes. The emission intensities of Eu[III] decrease due to the light interception by PNP. In the UV-visible spectra, a higher absorbance of PNP at the maximum excitation wavelength of Eu[III] indicates a more intense competition of energy absorption, and thus a stronger quenching effect on the fluorescence intensity of Eu[III] can be expected.[17,59] As shown in Fig. 8b, the optical densities of PNP dispersed in ILs recorded at the corresponding excitation wavelength were all higher than that in water (0.640 at 288 nm). Hence, a more efficient quenching efficiency was achieved when Eu[III] was dispersed in ILs. Moreover, the absorption frequencies of n → π* electronic transitions of nitroaromatic compounds are known to increase with the polarity of the solvent.[64] Accordingly, the peak position of PNP dispersed in ILs was observed to red-shift as a consequence of the lower solvent polarity of the ILs compared to water.[65] Furthermore, this variation also facilitated more of a spectral overlap with the emission spectrum of Eu[III], which led to the re-absorption of the emitted light of Eu[III]. Therefore, a decrease in the emission intensity was observed. As verified from Fig. S7,† the area of spectral overlap for PNP and Eu[III] dispersed in ILs is mostly larger than that in water, thus a more efficient quenching efficiency and a higher sensitivity were achieved during the titration of Eu[III] dispersed in the ILs. In summary, the quenching process is a synergetic result of ground state electrostatic interactions and a favorable PET process, as well as a strong IFE.

Furthermore, the absorption spectra of PNP in aqueous solutions containing 10% ILs were also investigated and are shown in Fig. 8c. The optical densities of PNP recorded at 288 nm were in the same order as the quenching efficiencies obtained from the fluorescence quenching titrations. A relatively lower absorbance was observed for an aqueous solution containing 10%[Bmim]BF_4 and 10%[Hmim]Br, followed by 10%[Bmim]TfO, and particularly 10%[Bmim]TA. So, the lower quenching efficiency detected in aqueous solution containing 10% ILs could be explained as being the result of a poor IFE. Interestingly, a new absorption band was found to appear at 402 nm after the addition of 10%[Bmim]TfO and 10%[Bmim]TA, which could be ascribed to the decreased intermolecular H-bond interactions of PNP. As shown in the inset of Fig. 8c, the H-bonds were mainly formed between the nitro groups of PNP and the hydroxyl groups of water in aqueous solution. After the addition of the ILs, H-bonds were also formed between water molecules and the carboxyl and sulfonate groups of TA^- and TFO^-, thereby resulting in competition with the PNP. As a result of the relatively stronger hydrogen bonding ability of the ILs, the H-bond interaction between PNP and water decreased and almost disappeared when PNP was dispersed in aqueous solution containing ILs. Hence, the absorbance bands of PNP

shifted to a higher wavelength. It is worth noting that the reported hydrogen bonding abilities of TA^- and TFO^- are relatively stronger than those of Br^- and BF_4^-,[59] therefore meaning that the hydrogen bond interaction has less influence after the addition of [Bmim]BF_4 and [Hmim]Br. Therefore, no new bands were observed in aqueous solutions containing [Bmim]BF_4 and [Hmim]Br. Furthermore, the UV-vis absorption spectra and their corresponding emission spectra (Fig. S8†) showed that aqueous solutions containing 10% ILs had comparatively less overlap in their absorption bands with the ligand centered emission band of Eu[III].

4. Conclusions

In conclusion, we have studied the influence of imidazolium-based ILs on the fluorescence detection performance of PNP using a lanthanide-based fluorescent Eu[III] probe. The experimental results showed that the antenna effect and coordination structure of Eu[III] were affected by the ILs. Surprisingly, a high selectivity and sensitivity were obtained for Eu[III] toward [Bmim]NO_3 in aqueous solution. In addition, the quenching efficiency of Eu[III] for PNP detection was largely dependent on the types and content of the ILs. According to the results of the enhanced energy transfer effect of Eu[III], a more efficient detection performance was achieved in ILs than in water. The decreased detection performance of Eu[III] upon the addition of ILs at a content of 10% demonstrated that a more suitable solvent environment to Eu[III] could be supplied by pure ILs. UV-vis spectra revealed that the absorption of PNP was changed by the addition of ILs both in terms of peak intensity and position, which could be attributed to the decreased solvent polarity of the ILs. The mechanism of fluorescence quenching was proposed to be a synergistic effect of electrostatic interactions and PET, as well as IFE. It is hoped that this study will pave the way toward the detection of nitro compounds in non-traditional solvents and further broaden the application of lanthanide-based fluorescent probes.

Conflicts of interest

There are no conflicts of interest to declare.

Acknowledgements

We are thankful for the Science and Technology Innovation Program of the Higher Education Institutions of Shanxi Province, China (No. 2020L0142), the financial support from the National Natural Science Foundation of China (22002077) and the PhD Research Startup Foundation of Shanxi Agricultural University, China (No. 2017YJ36). We would also like to thank TopEdit (https://www.topeditsci.com) for its linguistic assistance during the preparation of this manuscript.

References

1 S. B. Khan, K. Akhtar, E. M. Bakhsh and A. M. Asiri, *Appl. Surf. Sci.*, 2019, **492**, 726.
2 A. Khoddami, M. A. Wilkes and T. H. Roberts, *Molecules*, 2013, **18**, 2328.
3 M. A. Shannon, P. W. Bohn, M. Elimelech, J. G. Georgiadis, B. J. Marinas and A. M. Mayes, *Nature*, 2008, **452**, 301.
4 J. Akhavan, *The Chemistry of Explosives*, Royal Society of Chemistry, Cambridge, 2004.
5 J. Chen, M. Song, Y. Li, Y. Zhang, K. Taya and C. Li, *Environ. Toxicol. Pharmacol.*, 2016, **41**, 266.
6 R. Madhu, C. Karuppiah, S. M. Chen, P. Veerakumar and S. B. Liu, *Anal. Methods*, 2014, **6**, 5274.
7 D. S. Moore, *Rev. Sci. Instrum.*, 2004, **75**, 2499.
8 P. Wu and X. P. Yan, *Chem. Soc. Rev.*, 2013, **42**, 5489.
9 Y. Salinas, R. Martínez-Máñez, M. D. Marcos, F. Sancenón, A. M. Costero, M. Parra and S. Gil, *Chem. Soc. Rev.*, 2012, **41**, 1261.
10 H. Cavaye, P. E. Shaw, X. Wand, P. L. Burn, S. C. Lo and P. Meredith, *Macromolecules*, 2010, **43**, 10253.
11 S. V. Eliseeva and J.-C. G. Bunzli, *Chem. Soc. Rev.*, 2010, **39**, 189.
12 J. Qin, B. Ma, X. Liu, H. Lu, X. Dong, S. Zang and H. Hou, *J. Mater. Chem. A*, 2015, **3**, 12690.
13 S. Wu, H. Min, W. Shi and P. Cheng, *Adv. Mater.*, 2019, **32**, 1805871.
14 J. D. Xiao, L. G. Qiu, F. Ke, Y. P. Yuan, G. S. Xu, Y. M. Wang and X. Jiang, *J. Mater. Chem. A*, 2013, **1**, 8745.
15 X. Z. Song, S. Y. Song, S. N. Zhao, Z. M. Hao, M. Zhu, X. Meng, L. L. Wu and H. J. Zhang, *Adv. Funct. Mater.*, 2014, **24**, 4034.
16 M. L. Han, G. X. Wen, W. W. Dong, Z. H. Zhou, Y. P. Wu, J. Zhao, D. S. Li, L. F. Ma and X. Bu, *J. Mater. Chem. C*, 2017, **5**, 8469.
17 P. Majee, D. K. Singha, S. K. Mondal and P. Mahata, *ChemistrySelect*, 2018, **3**, 683.
18 Z. Lei, B. Chen, Y. M. Koo and D. R. MacFarlane, *Chem. Rev.*, 2017, **117**, 6633.
19 M. Freemantle, *An Introduction to Ionic Liquids*, ed. T. Welton and R. D. Rogers, RSC Publishing, London, 2010.
20 Y. Qiao, W. Ma, N. Theyssen, C. Chen and Z. Hou, *Chem. Rev.*, 2017, **117**, 6881.
21 Q. Yang, Z. Zhang, X. G. Sun, Y. S. Hu, H. Xing and S. Dai, *Chem. Soc. Rev.*, 2018, **47**, 2020.
22 G. W. Meindersma, A. R. Hansmeier and A. B. de Haan, *Ind. Eng. Chem. Res.*, 2010, **49**, 7530.
23 P. Isosaari, V. Srivastava and M. Sillanpää, *Sci. Total Environ.*, 2019, **690**, 604.
24 C. D. Wilfred, C. F. Kiat, Z. Man, M. A. Bustam, M. I. M. Mutalib and C. Z. Phak, *Fuel Process. Technol.*, 2012, **93**, 85.
25 O. G. Sas, I. Domínguez, B. González and Á. Domínguez, *J. Environ. Manag.*, 2018, **228**, 475.
26 M. Cheng, J. Jiang, J. Wang and J. Fan, *ACS Sustainable Chem. Eng.*, 2019, **7**, 8195.
27 L. Zhang, Y. Ding, B. Long, L. Yao, H. Yuan and Y. Dai, *J. Mol. Liq.*, 2020, **312**, 113440.
28 S. A. Mohammed, N. Zouli and M. Al-Dahhan, *Desalin. Water Treat.*, 2018, **110**, 168.

29 Q. Al-Obaidi, M. Alabdulmuhsin, A. Tolstik, J. G. Trautman and M. Al-Dahhan, *J. Water Process. Eng.*, 2021, **39**, 101729.
30 G. Singh, M. Kaur and T. S. Kang, *J. Mater. Chem. A*, 2019, **7**, 5185.
31 S. R. Thawarkar, B. Thombare, B. S. Munde and N. D. Khupse, *RSC Adv.*, 2018, **8**, 38384.
32 K. Yao, C. Zhao, N. Wang, W. Lu, H. Wang, S. Zhao and J. Wang, *CrystEngComm*, 2018, **20**, 6328.
33 R. Su, F. Wang, J. Ding, Q. Li, W. Zhou, Y. Liu, B. Gao and Q. Yue, *Carbohydr. Polym.*, 2019, **220**, 202.
34 A. KhorsandKheirabad, X. Zhou, D. Xie, H. Wang and J. Yuan, *Macromol. Rapid Commun.*, 2021, **42**, 2000143.
35 N. Bhawawet, J. B. Essner, D. V. Wagle and G. A. Baker, *Langmuir*, 2017, **33**, 6029.
36 K. Binnemans, *Chem. Rev.*, 2007, **107**, 2592.
37 A. V. Mudring and S. Tang, *Eur. J. Inorg. Chem.*, 2010, **18**, 2569.
38 A. V. Mudring, A. Babai, S. Arenz, R. Giernoth, K. Binnemans, K. Driesen and P. Nockemann, *J. Alloys Compd.*, 2006, **418**, 204.
39 I. Billard, G. Moutiers, A. Labet, A. El Azzi, C. Gaillard, C. Mariet and K. Lützenkirchen, *Inorg. Chem.*, 2003, **42**, 1726.
40 P. Nockemann, E. Beurer, K. Driesen, R. Van Deun, K. Van Hecke, L. Van Meervelt and K. Binnemans, *Chem. Commun.*, 2005, **34**, 4354.
41 S. Yi, M. Yao, J. Wang and X. Chen, *Phys. Chem. Chem. Phys.*, 2016, **18**, 27603.
42 S. F. Tang, C. Lorbeer, X. Wang, P. Ghosh and A. V. Mudring, *Inorg. Chem.*, 2014, **53**, 9027.
43 Y. Han, C. Lin, Q. Meng, F. Dai, A. G. Sykes, M. T. Berry and P. Stanley, *May, Inorg. Chem.*, 2014, **53**, 5494.
44 K. Lunstroot, K. Driesen, P. Nockemann, C. Görller-Walrand, K. Binnemans, S. Bellayer, J. L. Bideau and A. Vioux, *Chem. Mater.*, 2006, **18**, 5711.
45 H. R. Li, Y. Wang, T. R. Wang and Z. Q. Li, in *Application of Ionic Liquids on Rare Earth Green Separation and Utilization*, ed. J. Chen, Springer-Verlag Berlin Heidelberg, 2016, pp. 157–178, ch. 7.
46 I. T. Weber, A. J. G. de Melo, M. A. D. M. Lucena, M. O. Rodrigues and S. Alves Junior, *Anal. Chem.*, 2011, **83**, 4720.
47 Q. Xu, Z. Li and H. Li, *Chem. -Eur. J.*, 2016, **22**, 3037.
48 J. Xu, T. Zhu, J. Shi, B. Song, L. Zhang, D. Zhao, X. Dong, N. Bi, J. Gou and L. Jia, *J. Rare Earths*, 2021, DOI: 10.1016/j.jre.2021.11.007.
49 L. Jia, X. Chen, J. Xu, L. Zhang, S. Guo, N. Bi and T. Zhu, *J. Hazard. Mater.*, 2021, **402**, 123776.
50 Q. li, L. Jin, L. Li, W. Ma, Z. Wang and J. hao, *J. Mater. Chem. C*, 2017, **5**, 4670.
51 M. R. George, C. A. Golden, M. C. Grossel and R. J. Curry, *Inorg. Chem.*, 2006, **45**, 1739.
52 S. M. Bruno, R. A. Ferreira, F. A. Almeida Paz, L. D. Carlos, M. Pillinger, P. Ribeiro-Claro and I. S. Gonçalves, *Inorg. Chem.*, 2009, **48**, 4882.
53 Y. F. Shao, B. Yan and Q. P. Li, *Eur. J. Inorg. Chem.*, 2013, **3**, 381.
54 K. Binnemans, *Coord. Chem. Rev.*, 2015, **295**, 1.
55 C. Görller-Walrand, L. Fluyt, A. Ceulemans and W. Carnall, *J. Chem. Phys.*, 1991, **95**, 3099.
56 N. Filipescu, W. F. Sager and F. A. Serafin, *J. Phys. Chem.*, 1964, **68**, 3324.
57 P. Li, Y. G. Wang, H. R. Li and G. Calzaferri, *Angew. Chem., Int. Ed.*, 2014, **53**, 2904.
58 P. A. Hunt, C. R. Ashworth and R. P. Matthews, *Chem. Soc. Rev.*, 2015, **44**, 1257.
59 X. H. Zhou, L. Li, H. H. Li, A. Li, T. Yang and W. Huang, *Dalton Trans.*, 2013, **42**, 5718.
60 Y. Q. Wang, Q. H. Tan, H. T. Liu and Z. L. Liu, *RSC Adv.*, 2015, **5**, 86614.
61 P. Dutta, D. Saikia, N. C. Adhikary and N. S. Sarma, *ACS Appl. Mater. Interfaces*, 2015, **7**, 24778.
62 A. S. Tanwar, S. Hussain, A. H. Malik, M. A. Afroz and P. K. Iyer, *ACS Sens*, 2016, **1**, 1070.
63 R. Sun, X. Huo, H. Lu, S. Feng, D. Wang and H. Liu, *Sens. Actuators, B*, 2018, **265**, 476.
64 H. McConnell, *J. Chem. Phys.*, 1952, **20**, 700.
65 L. Crowhurst, P. R. Mawdsley, J. M. Perez-Arlandis, P. A. Salter and T. Welton, *Phys. Chem. Chem. Phys.*, 2003, **5**, 2790.